Wan, Jingshu; Tao, Li; Wang, Baoyuan; Zhang, Jun; Wang, Hao; Lund, Peter D.

A facile method to produce TiO_2 nanorods for high-efficiency dye solar cells

Published in:
Journal of Power Sources

DOI:
10.1016/j.jpowsour.2019.227012

Published: 31/10/2019

Document Version
Peer-reviewed accepted author manuscript, also known as Final accepted manuscript or Post-print

Please cite the original version:
Wan, J., Tao, L., Wang, B., Zhang, J., Wang, H., & Lund, P. D. (2019). A facile method to produce TiO_2 nanorods for high-efficiency dye solar cells. *Journal of Power Sources*, *438*, 1-8. Article 227012. https://doi.org/10.1016/j.jpowsour.2019.227012

A facile method to produce TiO_2 nanorods for high-efficiency dye solar cells

Jingshu Wan[a], Li Tao [a]*, Baoyuan Wang [a], Jun Zhang[a]*, Hao Wang[a]*, Peter D. Lund[b]

[a] Hubei Key Laboratory of Ferroelectric and Dielectric Materials and Devices, Faculty of Physics and Electronic Science, Hubei University, Wuhan 430062, P.R. of China

[b] Department of Applied Physics, Aalto University, School of Science, P.O.Box 15100, FI-00076 Aalto, Espoo, Finland

*Corresponding authors: taoli1107@126.com (L.Tao); gwen_zhang@126.com (J. Zhang); nanoguy@126.com (H. Wang)

Abstract

Highly ordered TiO_2 nanorods are considered promising for photoanodes in dye-sensitized solar cells due to their high charge transfer rate of photo-generated electrons, but they often suffer from low specific area, which may lead to a low conversion efficiency. Here, we produce long vertical single-crystalline rutile TiO_2-nanorod arrays on FTO by the hydrothermal method. To further increase the specific area, the TiO_2-nanorod arrays are etched in a secondary hydrothermal process by hydrochloric acid. The etching time have a major effect on the nanorod microstructure and on the dye-sensitized solar cells efficiency. The best result is reached with 8 hours of etching, which resulted in a record high conversion efficiency of 11.14 ± 0.12 % (certified efficiency 10.3%) under AM 1.5 conditions. The record cell has an open voltage of 0.79 V and a short current density of 21.59 mA/cm^2. The proposed manufacturing approach of TiO_2 nanorods is

highly potential for producing high-efficiency dye-sensitized solar cells.

Key Words: Dye-sensitized solar cells; TiO_2 nanorods; hydrothermal processing, etching

Introduction

The dye-sensitized solar cell (DSSC) is potential solar cell technology, which has intensively been investigated during the last two decades [1-3]. The highest efficiency of DSSC reported so far is close to 15% [4]. A DSSC is typically made up of a mesoporous film of metal oxide semiconducting nanoparticles (e.g. TiO_2) covered with a monolayer of dye molecules on a conducting substrate (e.g. FTO glass) forming a photo-anode, a counter electrode, and a redox electrolyte. The performance of DSSC is strongly affected by the photo-anode through the charge transfer process of photoelectrons from the excited dye molecules collected and transported by the semiconductor nanoparticles to the conductive substrate [5-10]. Compared to traditional TiO_2-nanoparticle photo-anodes, one-dimensional ordered TiO_2-nanorod arrays (NRA) have unique advantages such as a direct pathway for electron transfer with less grain boundaries and high light adsorption due to the light trapping effect [11-19]. Furthermore, highly crystalline TiO_2 NRAs can directly be fabricated on transparent FTO substrates by the wet chemical or hydrothermal method [17, 20-24]. However, the reported power conversion efficiency (PCE) of DSSCs with ordered TiO_2-nanorod array photo-anodes has been relatively low due to insufficient dye loading on the photo-anode surface because of low specific area of TiO_2 NRAs (2-5 μm)[20, 25, 26].

To address the issue of a low specific area, two strategies have typically been proposed. First, nanoparticles can be introduced on TiO_2-NRA photo-anodes. Second, the length of the TiO_2 NRAs can be increased. For the first strategy, decorated TiO_2 nanorods arrays (TNAs) with TiO_2 nanoparticles (TNPs) have been introduced through $TiCl_4$ treatment[27-31] or through electrostatic deposition by polymeric material[32]. A drawback of these methods is that TiO_2 nanoparticles often just cover the top part of the TiO_2 nanorods or may even for conglomerates on the top surface of the TNAs, which could be somewhat mitigated by TNA/TNP-bilayer photo-anodes [8, 19, 27-31, 33-35]. However, controlling the interface between the bilayers is important to reach a high PCE [34]. The second strategy to enhance the specific area is to increase the length of the nanorods [34]. Photo-anodes with 30 μm [36] and 47μm [35] long TiO_2-nanowire arrays have been prepared on FTO by a multi-step hydrothermal method. However, ultra-long TiO_2 NRAs have a relative compact bottom layer, which may prevent the dye molecules to penetrate. In addition, such ultra-long NRAs may disconnect from the substrate during the hydrothermal growth and device fabrication. To our best knowledge, the highest efficiency of DSSCs with TiO_2 NRAs is 7.91% [36].

In this paper, we report of an alternative route to fabricate highly ordered single-crystalline rutile TiO_2 NRAs on a transparent FTO substrate using the hydrothermal method. The length of TiO_2 NRAs can be controlled by adjusting the concentration of $TiCl_4$ in the reaction solution and by the time of hydrothermal growth. Moreover, the peeling-off of the NRAs from the FTO substrate was successfully solved by precisely controlling the heating and cooling rate during the annealing treatment of the TiO_2-NRA film. A simple hydrochloric acid treatment was used to etch the TiO_2 NRAs to improve the dye loading. TiO_2 NRAs etched for 8 hours resulted in a lower electron transfer resistance, prolonged electron lifetime, and good dye loading. DSSCs fabricated from optimized TiO_2-NRAs reached a high PCE of 11.14% (certified value 10.3%), which is the highest ever reported efficiency for this type of DSSC.

Experimental

Preparation of TiO_2 nanorods arrays

Titanium tetrachloride ($TiCl_4$) and hydrochloric acid (HCl 36.5-38 wt%) were obtained from Sinopharm Chemical Reagent Co., Ltd., China. 4-tert-butylpyridine (TBP) was purchased from Xi′an Polymer Light Technology Corp. All chemicals were used without further purification.

2 cm by 2 cm commercial FTO glass was ultrasonically cleaned in acetone, deionized (DI) water, and ethanol for 30 min in turn. Then the cleaned FTO was directly immersed into a 0.3M $TiCl_4$ aqueous solution at 70 ℃ for 2 h. After completion, the modified FTO was fully rinsed by deionized water followed by annealing at 500℃ for 1 h to obtain a seed layer.

Rutile TiO_2 NRAs were directly grown on the FTO with a seed layer using a hydrothermal synthesis method. 1-5 ml $TiCl_4$ was slowly dropped into the mixture which contained 30 ml hydrochloric acid and 30 ml deionized water. The reaction solution was stirred continuously for at least 2 h in air to get a transparent solution, after which the solution was poured into a Teflon-lined container with a seed layer at 150℃ for 10-12 h.

The TiO_2 NRAs were rinsed with deionized water to remove the residual and finally annealed at 500℃ for 2 h under strict control of the heating and cooling rate.

Hydrochloric acid etching toward TiO_2 nanorods arrays

A solution of 30 ml HCl and 30 ml deionized water was poured into the Teflon-lined container followed by hydrothermal etching at 150℃ for 6-10 h. After the container had cooled down to room temperature, the samples were washed in deionized water followed by annealing at 500℃ for 2 h controlling the heating and cooling rate.

Assembling of DSSCs

The modified TiO_2 NRAs were immersed into 0.5 mM of N719 dye for 12 h with an active area of 0.125 cm^2. The photo-anode sensitized by the dye was assembled with a Pt-FTO substrate (counter electrode) in a sandwich configuration and filled up by the electrolyte, which was composed of 0.03M I_2, 0.1M guanidiniumthiocyanute(GuSCN), 0.5M 4-tert-butylpyridine（TBP, and 0.6M 1-methyl-3-propylimidazolium iodide (BMII) in an acetonitrile and valeronitrile solution. Each cell group tested here consisted of 5 samples, and each group of cells was measured over 10 times to yield the measurement outcome.

Characterization and measurements

The morphology of the TiO_2 NRAs was determined with SEM (FESEM, JEOL JSM-7100F) and TEM (JEOL JEM 2010). A X-ray diffractometer (XRD, Brucker D8) was used characterize the microstructure of TiO_2 NRAs. A UV-vis spectrophotometer (UV-3600, Shimadzu) was used to determine the dye loading, light absorption and reflectance vs wavelength. The Pt-film on the FTO glass substrate (counter electrode) was sputtered using a magnetron sputtering system (Japan ACS-400-C4). The photovoltaic parameters (*J-V*-curves) of the solar cells were determined with a digital multimeter (Keithley 2402) under AM1.5G 100 mW/cm^2 illumination using a solar simulator (Newport). The electrochemical impedance spectrum (EIS) of the DSSCs was recorded with an electrochemical workstation (CHI-660D) at open circuit with a 10 mV AC signal over a frequency range of 0.1–10^5 Hz under dark condition. Nitrogen adsorption-desorption isotherms were carried out on Mike Merck ASAP2020 to give the specific area of the photo-anodes.

Results and discussion

Figure 1 (a)-(d) shows how the etching time affects the gap between adjacent TiO_2 nanorods. The diameter of the unetched TiO_2 nanorods is 100-200 nm. Several step edges are found on the top of the nanorods, which can serve as substrate for further growth of sub-nanorods. All nanorods show a regular shape of tetragonal pillar which is in agreement with literature [17, 29, 39, 40]. The etched samples clearly demonstrate a larger gap between the nanorods than the unetched ones, also decreasing the number of thick nanorods. The diameter of the etched nanorods decreased to 50-80 nm. Lateral morphology changes in the TiO_2 nanorods with 0 h and 8 h etching time are shown in Fig.

1 (e-h). The unetched TiO_2 NRAs vertically grown on the FTO substrate are highly ordered with a length of ~14.6 µm, but the seed layer is too thin to be distinguished from the NRAs. Also, the top and bottom of the NRAs are compact (Fig.1f). However, through hydrochloric acid etching treatment, both the top and the bottom of the TiO_2 NRAs become loose and the space of the top etched TiO_2 nanorods becomes enlarged. However, the etching treatment does not influence the length of the TiO_2 nanorods. The enlargement of the surface area by the hydrochloric acid etching thus happens without sacrificing the length of the TiO_2 nanorods. This can be explained as follows: the preferential etching plane of a rutile TiO_2 nanorod is the [001]-plane, in which direction the rutile TiO_2 nanorod dissolves preferentially decreasing the TiO_2 nanorod diameter. Moreover, the crystal defects of TiO_2 nanorods in the grain boundaries are favored sites for etching position. Therefore, the top portion of the densely packed TiO_2 nanorods arrays get split and become loose. However, when the etching time is over 10 h, the attachment between the TiO_2 NRAs and the FTO became unstable and the TiO_2 NRAs are easily peeled off from the FTO, which would decrease the charge transfer between the interface of TiO_2 NRAs and FTO, also verified by our EIS results discussed later.

The optimal etching time to maximize the surface area of TiO_2 NRAs, but still keeping the TiO_2 NRAs well attached on the FTO, was 8 hours. Below that (e.g. 3 hours) no significant changes at the top of the TiO_2 nanorods were found. Above that (e.g. 10 hours) the number of tiny NRAs would not increase, but the contact of the NRAs to the substrate would weaken. The increase in the specific area was also verified through the Brunauer Emmett Teller (BET) measurements.

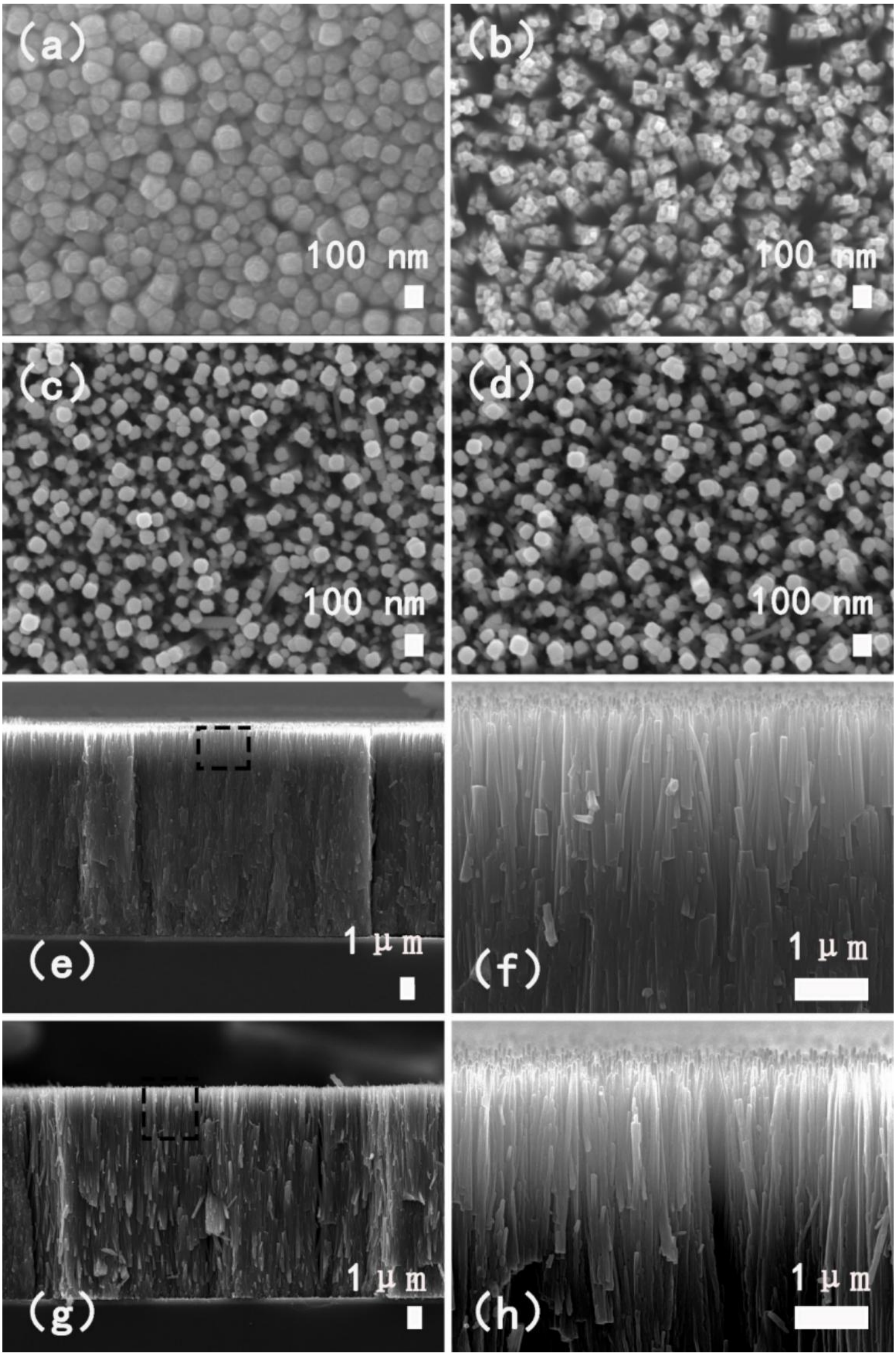

(a)
100 nm
(b)
100 nm
(c)
100 nm
(d)
100 nm
(e)
1 μm
(f)
1 μm
(g)
1 μm
(h)
1 μm

Figure 1. SEM plane image of TiO_2 nanorods etched for (a) 0 h, (b) 6 h, (c) 8 h, (d)10 h. Cross-sectional image of TiO_2 NRAs on FTO substrate etched for 0 h (e, f) and 8h (g, h).

The plane SEM of the etched TiO_2 nanorods in Fig.1 shows a significant change in the space between the TiO_2 nanorods, but the side wall changed after etching could not be detected. To further check if etching treatment may influence the side wall of nanorods, unetched and 8-h etched samples were peeled off from the FTO and analyzed by SEM in Fig. 2, which shows a lot of small TiO_2 nanoparticles on the surface of the unetched TiO_2 nanorods, but almost none on the etched sample.

Our experiment also revealed that TiO_2 NRAs were deposited on the both sides of the FTO and on the internal wall of the Teflon-lined container during the hydrothermal process. The hydrothermal reaction can be expressed as follows [23, 36, 41]:

$$TiCl_4 + H_2O \longrightarrow HCl + Ti(IV)complex \quad (1)$$

$$Ti(IV)complex \xrightarrow{dehydration} TiO_2 \quad (2)$$

Accordingly, $TiCl_4$ first hydrolyzes into a Ti(IV)-complex and is then dehydrated into TiO_2 under hydrothermal conditions. The growth process of the TiO_2 NRAs can be described as follows: firstly, nucleation starts with deposition of TiO_2 nanorods on the FTO, and then the nanorods start to grow based on nucleation. Using $TiCl_4$ as Ti^{4+} precursor may provide more Ti^{4+} for the TiO_2 NRAs growth process. On the other hand, the FTO substrate with a seed layer should provide plenty of nucleation sites for TiO_2 nanorods to grow so that the Ti^{4+} precursor quickly forms rutile TiO_2 nanorods on the

FTO substrate. The excessive Ti^{4+} precursor forms extra nucleation on the glass and the Teflon-lined container, which results in TiO_2 NRAs deposited on the reverse side of the FTO and on the Teflon-lined container wall. At the same time, a plenty of TiO_2 nanoparticles may be formed due to dehydration of the Ti(IV)-complex, and could be loaded on the surface of the TiO_2 nanorods. However, the 8-h etched TiO_2 NRAs had a uniform surface, which function as a fast electron transport pathway.

Figure 3 shows TEM and selected-area electron diffraction (SAED) images of the 8-h etched and unetched single nanorod. The SAED graphs (insets in Fig. 3 a and c) show the same single–crystal rutile structures and lattice fringes corresponding to the [110]-plane in the 8-h etched and unetched TiO_2 NRAs.

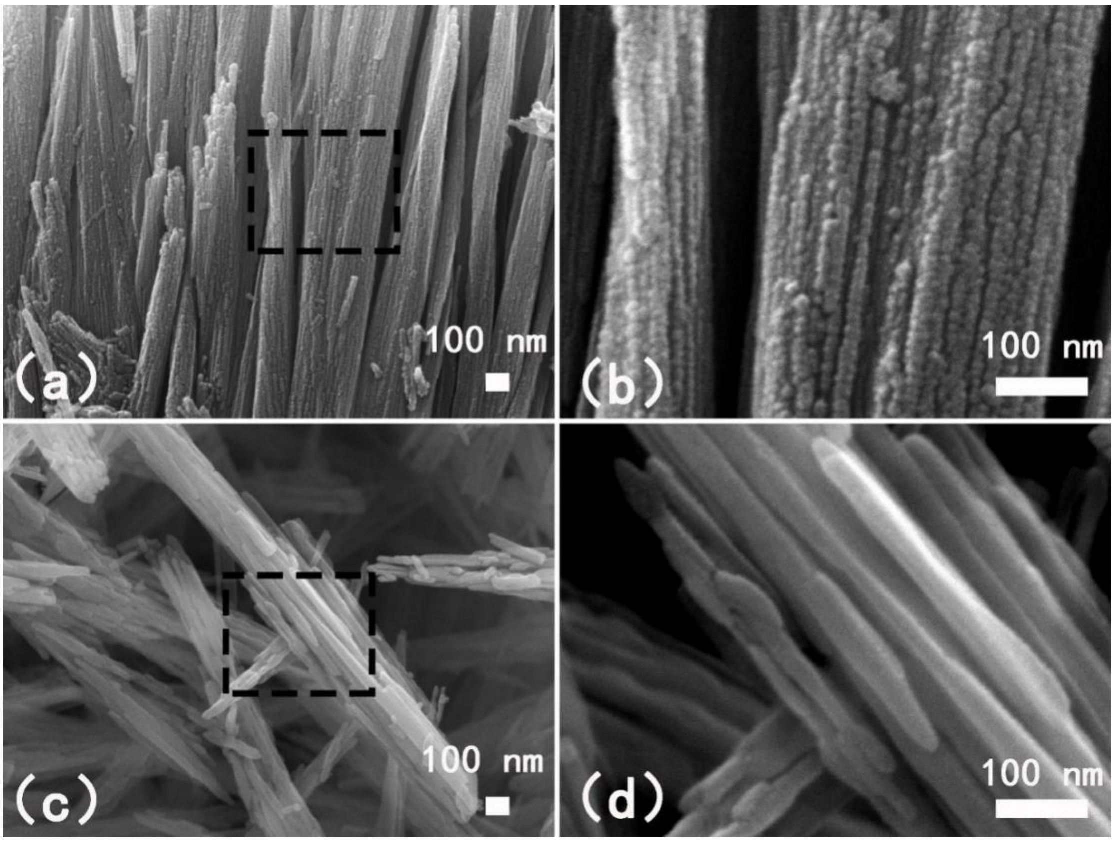

Figure 2 The SEM of the TiO_2 nanorods (a, b) and 8 h-etched TiO_2 nanorods (c, d).

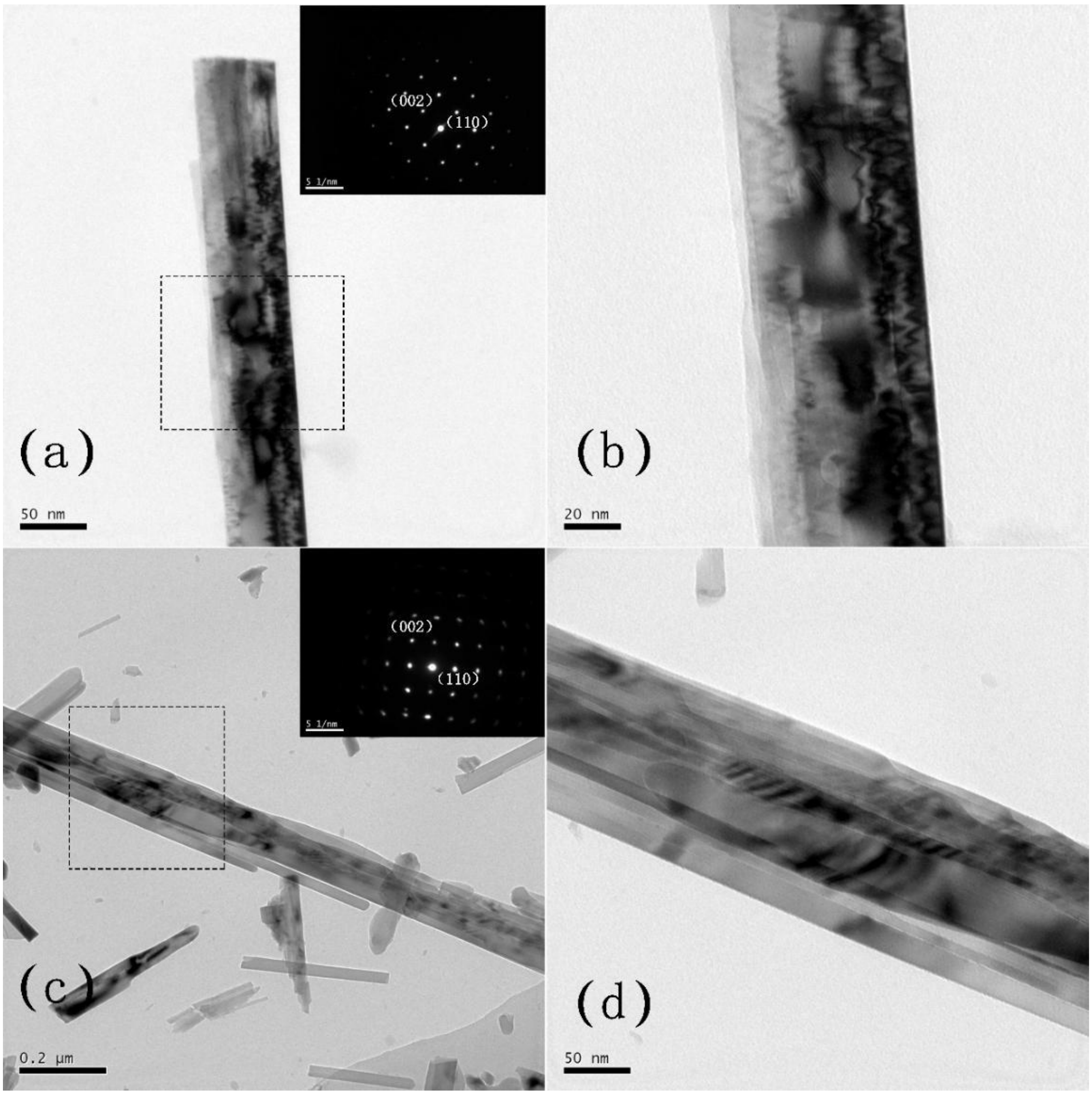

Figure 3. TEM and SAED of unetched (a, b) and 8-h etched TiO_2 nanorods (c, d).

To further confirm that the hydrochloric acid etching had no influence on the crystal structure of TiO_2 NRAs, XRD characterization was performed (Fig. 4). The (002) diffraction peak of TiO_2 NRAs at 62.9° (highest intensity) indicates a well ordered tetragonal rutile (JCPDS 87-0710), which is also verified by the cuboid shape of nanorods in the SEM images. The etched and unetched TiO_2 NRAs have the same diffraction peaks, though with differences in intensity, indicating that the etching treatment had no damage on the crystal structure of the TiO_2 NRAs. Based on the Scherrer equation, D= kλ/(Bcosθ), where λ is the wavelength of X radiation and k is 1.54 Å, the diameter of the TiO_2 nanorods should be 49.04 nm, 42.08 nm, 28.62 nm, and 26.31 nm, respectively, when the etching time is 0 h, 6 h, 8 h, and 10 h. This indicates that the diameter of the TiO_2 nanorods decrease with increasing etching time, also decreasing the intensity of the diffraction peaks.

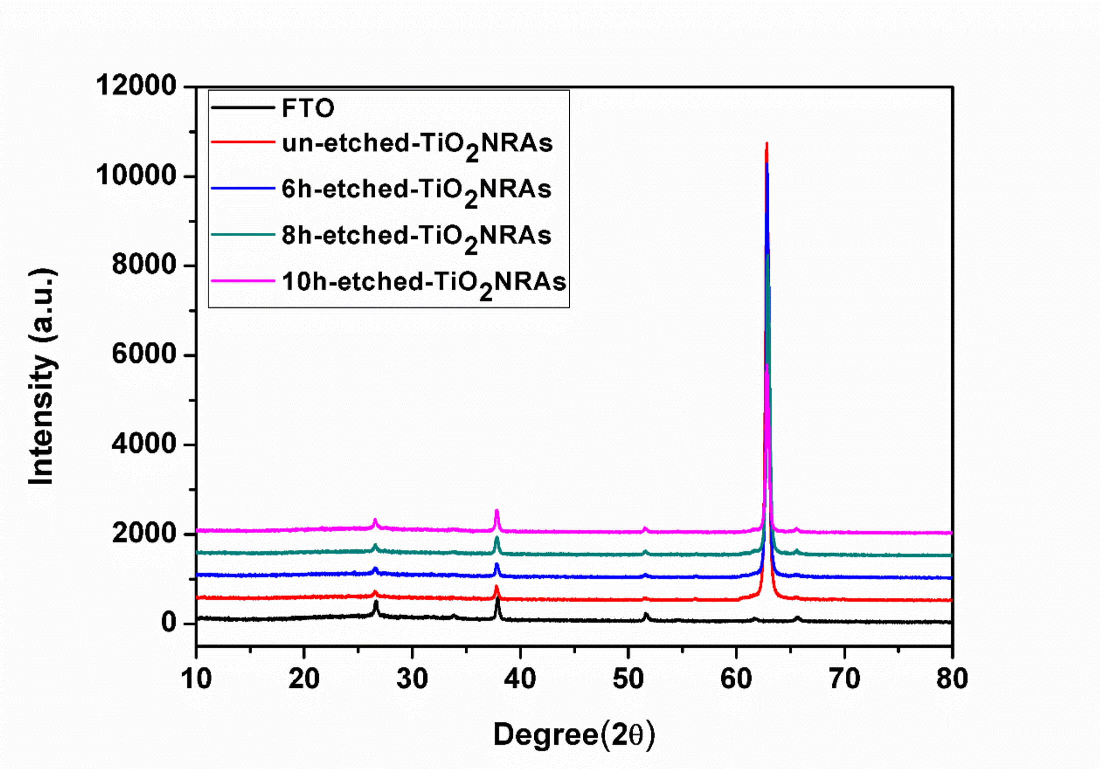

Figure 4. XRD patterns of the TiO_2 nanorods with different etching times.

The UV-vis absorption spectra of the TiO_2 film with and without the dye (N719) loading are shown in Fig. 5 (a) and (b). Both the etched and un-etched TiO_2 NRAs have an absorption edge at about 410 nm, which indicates a band gap of 3.02 eV. This is slightly less than the standard value of 3.20 eV for TiO_2, which is may partly be explained by quantum size effects of TiO_2 nanoparticles [42-44]. After dye adsorption, the absorption edge of the photo-anode shifts to 550 nm, which corresponds to the absorption edge of the N719 dye, thus demonstrating efficient photosensitization. The absorption intensity of the TiO_2 NRAs film after dye loading enhances when extending the etching time from 6 h to 8 h, but moving to 10 h decreases, the intensity little. The reason for better light harvesting ability of the photo-anode enhancing a 8-h etching time is due to the larger specific area of the TiO_2 NRAs film. At 10 h etching, the contact between the TiO_2 nanorods and FTO becomes unstable leading to some nanorods falling off from the FTO substrate when immersing the TiO_2-NRA film into the dye solution. Thus, the best light absorptance was achieved with a 8-h etched TiO_2 NRA.

The harvesting efficiency of incident light also depends on the light-scattering properties of the photo-anode, which can be estimated from the diffuse reflectance spectrum. A high reflectance to incident light indicates a high probability for capturing the incident light, which in turn could lead to improved short-circuit current density (Jsc). Fig. 5 (c) shows the light-scattering of unetched/etched TiO_2 nanorods between 400 nm and 700 nm. The 8-h etched sample had the highest diffuse reflectance in the visible light range, which should result in the best light absorption ability[45, 46].

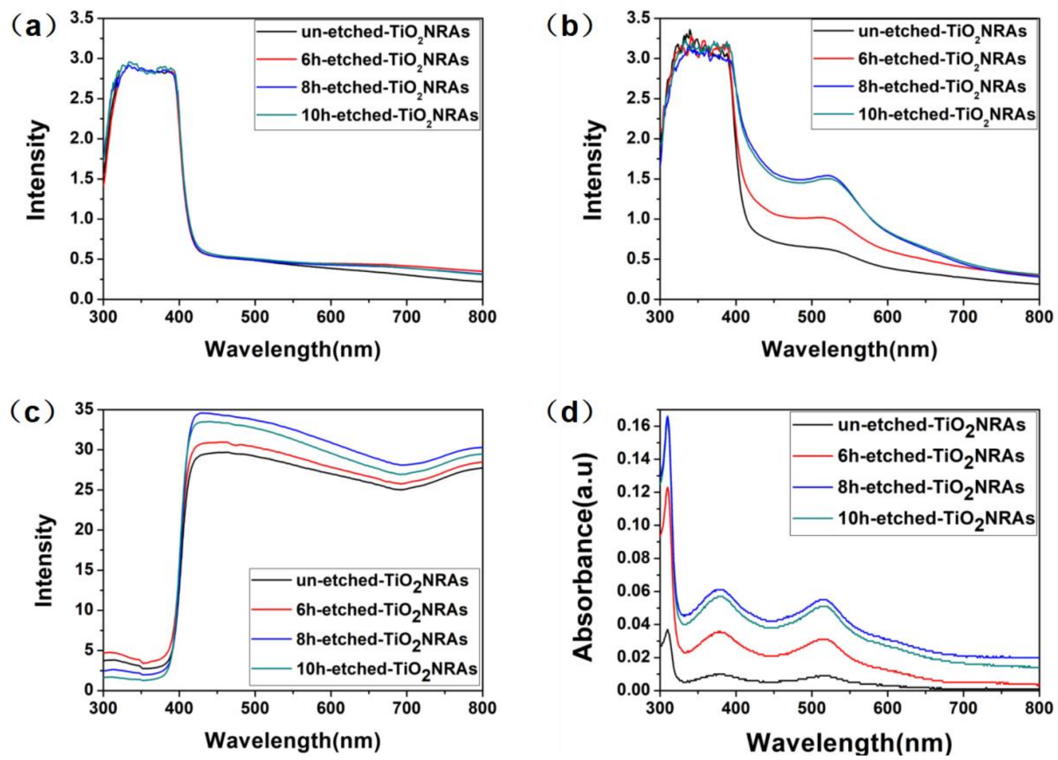

Figure 5. UV-vis absorption of the TiO_2 photo anode (a) before and (b) after dye absorption (b); (c) diffuse reflectance spectra of the TiO_2 photo anode; (d) dye absorption spectra of TiO_2 NRAs' saturation adsorption (d).

The photocurrent (J_{sc}) is closely related to the dye-loading ability of the photo-anode (Fig. 5(b)). The more the photo-anode surface can adsorb dye, the more photo-generated excitations will be produced, which may result in a higher photocurrent. The absorbance spectra of the dye desorption solution can be used to calculate the dye-loading from the Lambert–Beer law A =KCL, where A is the absorbance of the N719 dye desorption solution at 520 nm, L is the length of the cuvette used for the absorbance spectra measurement, K is the molar extinction coefficient of N719 at 520 nm equal to 1.41×10^4 $dm^3\ mol^{-1}\ cm^{-1}$. The dye saturation adsorption films were desorbed by 0.1 M NaOH alcohol aqueous solution for 12 h at room temperature under dark. Figure 5（d）shows the light absorption curves of these dye desorption solutions. All dye solutions have three absorption peaks at 310 nm, 380 nm, and 520 nm, respectively, in accordance to the light absorption features of the N719 dye [47, 48]. The calculated dye-loading of unetched/etched-TiO_2 NRAs is shown in Table 2, which shows that the absorption intensity of the dye-desorbed solution from etched-TiO_2 NRAs gradually increase in the visible region. There are two reasons for this phenomenon: First, the hydrochloric acid etching can efficiently roughen the surface and enlarge the specific area of the TiO_2 NRAs, which would adsorb more dye; second, hydrochloric acid etching treatment can lead to adsorption of hydroxyl (-OH) groups on the surface of the TiO_2 film [49]. Hydroxyl groups on the TiO_2 film surface can improve the dye loading of the TiO_2 photo-anode, because carboxylic anchoring groups residing on the dye molecules can interact with hydroxyl groups adsorbed on the TiO_2 surface [37, 50-53]. Therefore, the 8-h etched TiO_2 NRAs can better adsorb dye leading to a dye loading of 257.62 nmol cm^{-2} compared to 38.3 nmol cm^{-2} of the unetched sample. This indeed confirms that 8 hours of hydrothermal etching of TiO_2 NRAs is a very efficient way to enlarge the specific area [15, 17, 36, 39, 54]. The BET measurement shown in Fig. 6 and values in Table 2 indicate an increase in the surface area from 0.77 to 18.6 m^2g^{-1} when the etching time increases from 0 to 8 h.

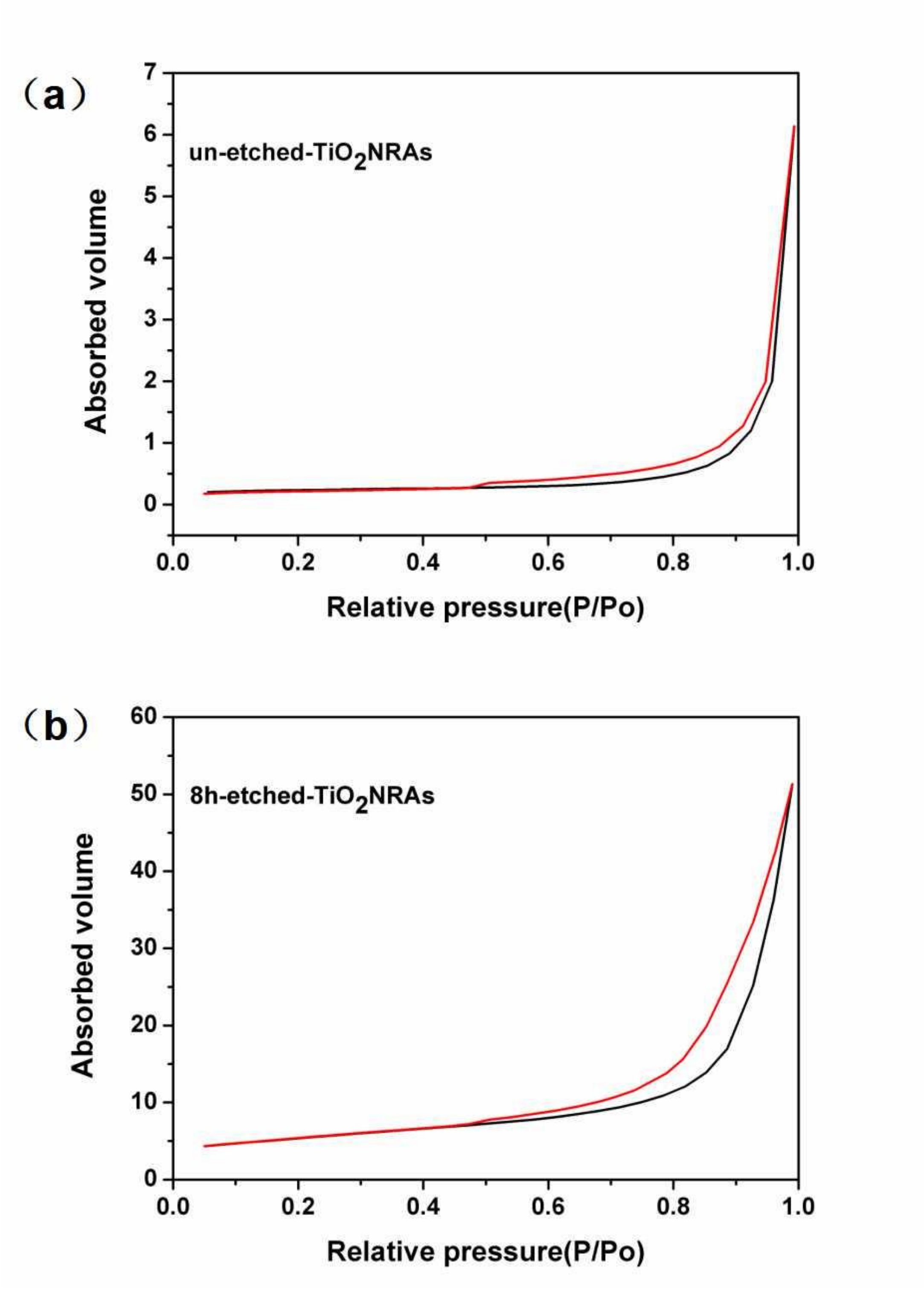

Figure 6. Nitrogen adsorption−desorption isotherms of the TiO_2 nanorods. (a) unetched and (b) 8-h etched TiO_2 nanorods.

We also performed EIS characterization to quantify the charge transfer resistance in the DSSCs studied. The equivalent circuit used is shown in the inset in Fig. 7(a). The sheet resistance (R_s) of the FTO substrates and the contact resistance between the FTO and TiO_2 is at the inception of the x-axis; the semicircle in high frequency region corresponds to the charge transfer resistance at the electrolyte/Pt-electrode interface (R_{pt}); the second semicircle is related to electron transfer at the interface between the photoanode/electrolyte (R_{ct}), and the third semicircle in the low frequency region corresponds to the characteristics of electron diffusion of the I^-/I_3^- redox couple. From Fig. 7 we see that the cells based on unetched and etched TiO_2 NRAs have almost same R_s and R_{pt} values due to the same electrolyte and counter electrodes used in these devices. The electron transport resistance R_{ct} (Table 1) decreases from 561.3 Ω to 12.48 Ω when changing unetched to etched TiO_2 NRAs in the DSSC, demonstrating faster electron transfer in the etched case. This is attributed to the highly aligned nanorods, which can serve as efficient transport path for electrons in the photo-anode and suppress charge recombination.

Figure 7(b) shows the Bode phase plots linked to the Nyquist plots. We can estimate from the EIS model the lifetime of the injected electrons in the photo-anode: $\tau_n=\omega_{max}^{-1} = (2\pi f_{max})^{-1}$, where f_{max} is the maximum frequency of the intermediate frequency range. As shown in Table 1, τ_n increases sharply from 1.46 ms to 30.8 ms when etching time is increased from 0 to 8 hours. A lower electron transfer resistance and prolonged electron lifetime improves the J_{sc} and V_{oc}.

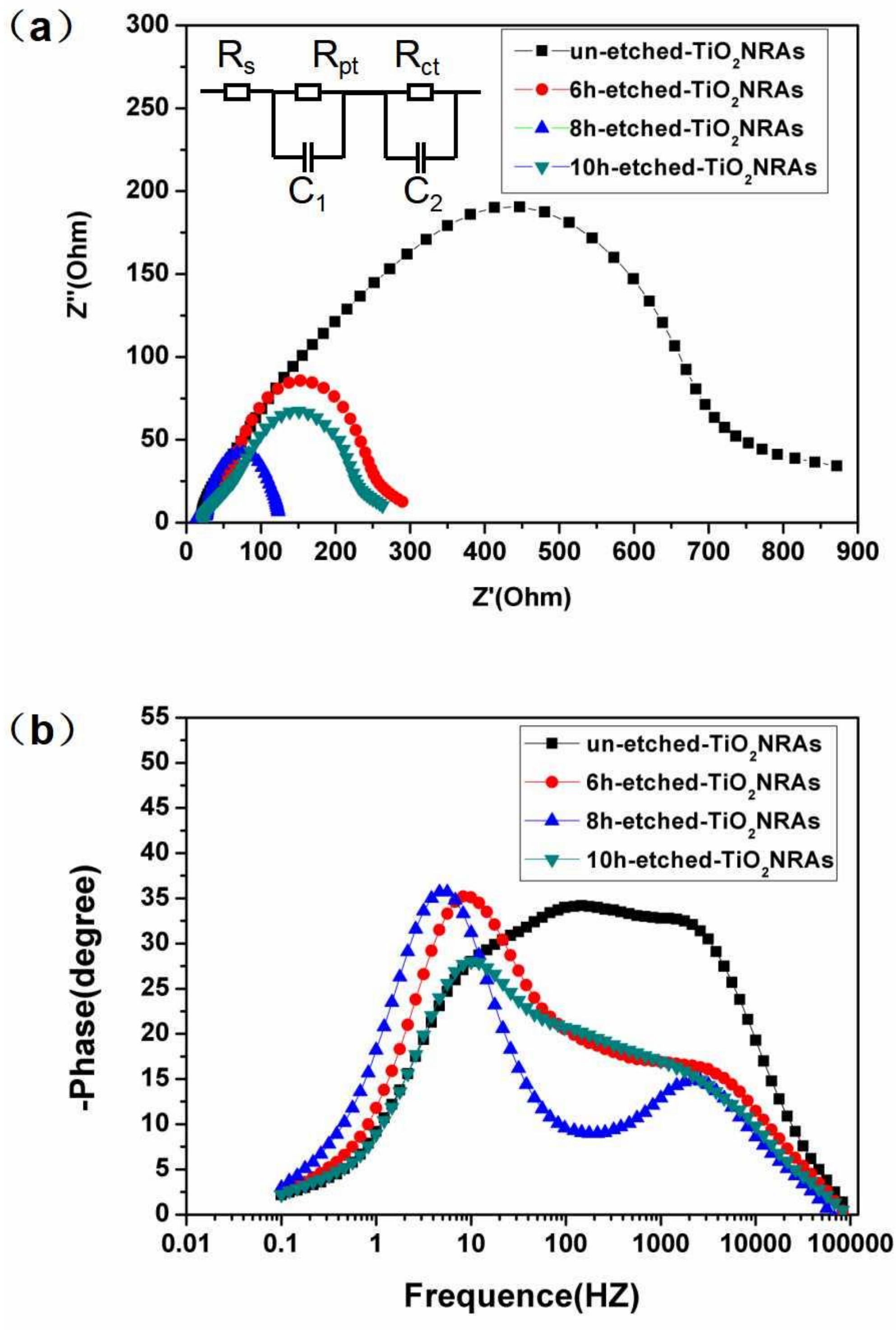

Figure 7. (a) Nyquist plots and (b) corresponding Bode phase plots of DSSCs with TiO_2 nanorods (NRA).

The current density-voltage (J-V) curves of the DSSCs with unetched/etched TiO_2 NRAs under AM1.5 illumination are shown in Fig. 8 and the corresponding photovoltaic parameters are summarized in Table 2. The unetched TiO_2-NRA-based DSSC has a low PCE of 1.34% (J_{sc}=3.65 mA/cm^2, FF=47.89%, V_{oc}=0.75V). Etching the TiO_2 nanorods improved the FF, J_{sc}, and V_{oc} of the cells. The best result was obtained with an 8-hour etching time which yielded a PCE of 11.14% (certified value 10.3%, see Supporting Information). The parameters of this DSSC were J_{sc}=21.59 mA/cm^2, FF=65.2%, and V_{oc}=0.79V. To our best knowledge, this is the highest ever-reported efficiency for this type of DSSC with 1-D TiO_2 nanorods.

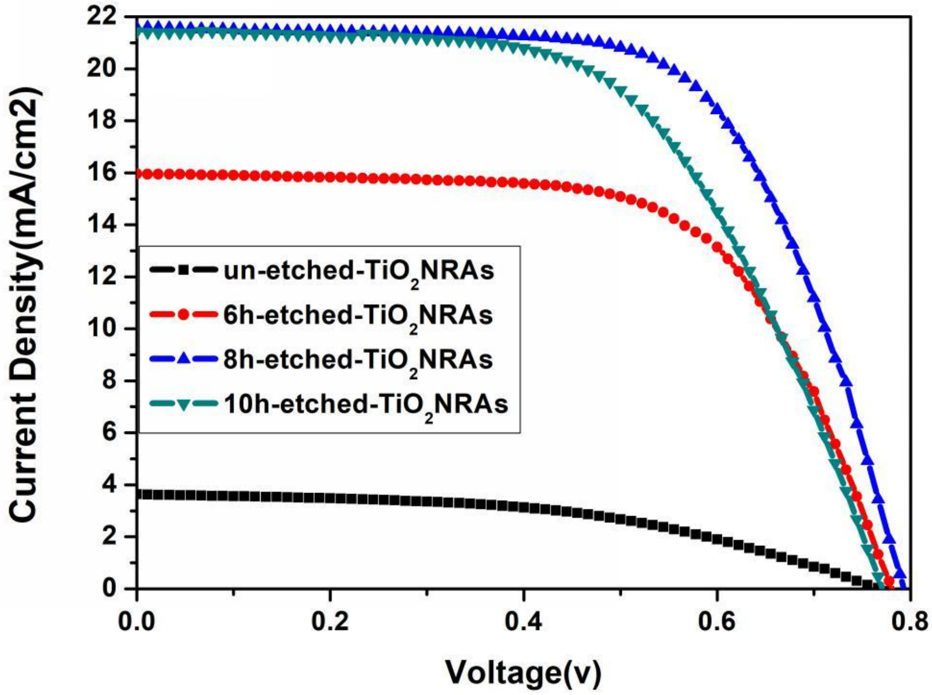

Figure 8. J-V curves of DSSCs under AM 1.5G 100 mW/cm^2.

Table 1. Sheet resistance (R_s), resistance of photoanode/electrolyte interface (R_{ct}), and lifetime of injected electrons (τ_n) versus etching time.

Cell	$R_s(\Omega)$	$R_{ct}(\Omega)$	τ_n (ms)
DSSC-0h	22.51	561.3	1.46
DSSC-6h	19.12	27.77	17.57
DSSC-8h	13.64	12.48	30.80
DSSC-10h	24.84	35.27	14.74

Table 2. Photovoltaic parameters, BET specific area, and dye-loading of DSSCs versus etching time of the TiO_2 nanorods.

Sample	DSSC-0h	DSSC-6h	DSSC-8h	DSSC-10h
Specific area (m^2g^{-1})	0.77	______	18.6	______
Dye adsorption (nmol cm^{-2})	38.30 ± 2.52	131.92 ± 1.89	257.62 ± 1.20	234.04 ± 3.35
V_{oc} (V)	0.7 6± 0.02	0.78 ± 0.01	0.79 ± 0.01	0.77 ± 0.02
J_{sc} (mA/cm^2)	3.65 ± 0.54	15.98 ± 0.37	21.59 ± 0.14	21.45 ± 0.47

FF (%)	47.89 ± 4.12	63.82 ± 2.46	65.2 ± 1.38	58.32 ± 2.96
PCE (%)	1.34 ± 0.46	7.95±0.24	11.14 ± 0.12	9.64 ± 0.34

Conclusions

Long single-crystalline rutile TiO_2 nanorods (NRA) were prepared by a simple hydrothermal synthesis method. We successfully solved the peeling off of NRAs from the substrate through adding a seed layer on the FTO and accurately controlling the heating and cooling rate. The length of the TiO_2 NRAs can be controlled by adjusting the amount of $TiCl_4$ in the reaction solution and through the growth time. DSSCs with unetched TiO_2 NRAs showed poor dye loading and a low PCE of 1.34%. Whereas TiO_2 NRAs etched in hydrochloric acid for 8 hours reached an excellent PCE of 11.14% under AM 1.5 illumination. This is the highest ever-reported efficiency value for this type of DSSC. The optimized TiO_2 NRAs showed a high specific area for dye loading, a high light harvesting efficiency, a lower electron transfer resistance, and a prolonged electron lifetime in the photo-anode. Our work represents a potential processing strategy to improve the efficiency of DSSCs with TiO_2 nanorod arrays.

Acknowledgements

This work was supported by the National Nature Science Foundation of China (No. 11874143 and 51602095).

References

[1] B. O'regan, M. Grätzel, Nature, 353 (1991) 737-740.

[2] M. Grätzel, Nature, 414 (2001) 338-344.

[3] W. Guo, C. Xu, G. Zhu, C. Pan, C. Lin, Z.L. Wang, Nano Energy, 1 (2012) 176-182.

[4] K. Kenji, A. Yohei, Y. Toru, O. Keiji, F. Jun-Ichi, H. Minoru, Chemical Communications, 51 (2015) 15894.

[5] N. Robertson, Angewandte Chemie International Edition, 45 (2006) 2338-2345.

[6] M. Grätzel, Accounts of Chemical Research, 42 (2009) 1788-1798.

[7] A. Hagfeldt, G. Boschloo, L. Sun, L. Kloo, H. Pettersson, Chemical Reviews, 110 (2010) 6595-6663.

[8] S.A. Arote, V.A. Tabhane, H.M. Pathan, Optical Materials, 75 (2018) 601-606.

[9] K. Zouhri, Renewable Energy, (2018) S0960148118303562.

[10] A.H. Ahliha, F. Nurosyid, A. Supriyanto, T. Kusumaningsih, Materials Science & Engineering Conference Series2018, pp. 012018.

[11] J. Zhang, L.I. Siqian, H. Ding, L.I. Quantong, B. Wang, X. Wang, H. Wang, Journal of Power Sources, 247 (2014) 807-812.

[12] K. Zhu, N.R. Neale, A. Miedaner, A.J. Frank, Nano Letters, 7 (2007) 69.

[13] D. Kim, A. Ghicov, S.P. Albu, P. Schmuki, Journal of the American Chemical Society, 130 (2008) 16454-16455.

[14] B. Wang, H. Ding, H.U. Yunxia, H. Zhou, S. Wang, T. Wang, R. Liu, J. Zhang, X. Wang, H. Wang, International Journal of Hydrogen Energy, 38 (2013) 16733-16739.

[15] X. Wang, R. Liu, T. Wang, B. Wang, Y. Xu, H. Wang, Applied Materials & Interfaces, 5 (2013) 3312-3316.

[16] Y. Hu, B. Wang, J. Zhang, T. Wang, R. Liu, J. Zhang, X. Wang, H. Wang, Nanoscale Research Letters, 8 (2013) 1-5.

[17] J. Wan, R. Liu, Y. Tong, S. Chen, Y. Hu, B. Wang, Y. Xu, H. Wang, Nanoscale research letters, 11 (2016) 1-9.

[18] J.B. Baxter, E.S. Aydil, Applied Physics Letters, 86 (2005) 053114-053114-053113.

[19] M.K. Ahmad, C.F. Soon, N. Nafarizal, A.B. Suriani, A. Mohamed, M.H. Mamat, M.F. Malek, M. Shimomura, K. Murakami, Journal of the Australian Ceramic Society, (2018) 1-8.

[20] B. Liu, E.S. Aydil, Journal of the American Chemical Society, 131 (2009) 3985.

[21] M. Lv, D. Zheng, M. Ye, L. Sun, J. Xiao, W. Guo, C. Lin, Nanoscale, 4 (2012) 5872-5879.

[22] H. Zhang, X. Liu, Y. Li, Q. Sun, Y. Wang, B.J. Wood, P. Liu, D. Yang, H. Zhao, Journal of Materials Chemistry, 22 (2012) 2465-2472.

[23] W.-Q. Wu, Y.-F. Xu, C.-Y. Su, D.-B. Kuang, Energy & Environmental Science, 7 (2014) 644-649.

[24] Y.Y. Li, J.G. Wang, H.H. Sun, B. Wei, ACS Applied Materials & Interfaces, 10 (2018) 11580.

[25] F. Li, S.J. Hu, L.D. Wei, B. Chi, L. Jian, Key Engineering Materials, 680 (2016) 278-281.

[26] X. Feng, K. Shankar, O.K. Varghese, M. Paulose, T.J. Latempa, C.A. Grimes, Nano Letters, 8 (2008) 3781-3786.

[27] W.Q. Wu, B.X. Lei, H.S. Rao, Y.F. Xu, Y.F. Wang, C.Y. Su, D.B. Kuang, Scientific Reports, 3 (2013) 1352.

[28] S.M. Wang, W.W. Dong, R.H. Tao, Z.H. Deng, J.Z. Shao, L.H. Hu, J. Zhu, X.D. Fang, Journal of Power Sources, 235 (2013) 193-201.

[29] W.Q. Wu, H.S. Rao, H.L. Feng, H.Y. Chen, D.B. Kuang, C.Y. Su, Nano Energy, 9 (2014) 15-24.

[30] M.K. Ahmad, V.M. Mohan, K. Murakami, Journal of Sol-Gel Science and Technology, 73 (2015) 655-659.

[31] J. Khamwannah, Y. Zhang, Y.N. Sun, H. Kim, C. Frandsen, S.D. Kong, S. Jin, Nano Energy, 1 (2012) 411-417.

[32] L. Zhaoyue, Z. Xintong, N. Shunsuke, J. Ming, D.A. Tryk, M. Taketoshi, F. Akira, Langmuir the Acs Journal of Surfaces & Colloids, 23 (2007) 10916-10919.

[33] H. Wang, B. Wang, J. Yu, Y. Hu, C. Xia, J. Zhang, R. Liu, Scientific Reports, 5 (2015).

[34] I. Ahmed, A. Fakharuddin, Q. Wali, A.R.B. Zainun, J. Ismail, R. Jose, Nanotechnology, 26 (2015) 105401.

[35] N.I. Beedri, P.K. Baviskar, A.T. Supekar, Inamuddin, S.R. Jadkar, H.M. Pathan, International Journal of Modern Physics B, (2018) 1840046.

[36] M. Lv, D. Zheng, M. Ye, J. Xiao, W. Guo, Y. Lai, L. Sun, C. Lin, J. Zuo, Energy & Environmental Science, 6 (2013) 1615-1622.

[37] T. Liu, B. Wang, J. Xie, Q. Li, J. Zhang, M.I. Asghar, P.D. Lund, H. Wang, Applied Surface Science, 355 (2015) 256-261.

[38] J. Zhang, Q. Li, S. Li, W. Yi, Y. Cong, P. Ruterana, W. Hao, Journal of Power Sources, 268 (2014)

941-949.

[39] B. Wang, J. Wan, Q. Liu, J. Zhang, H. Wang, RSC Advances, 5 (2015) 82968-82976.

[40] W.Q. Wu, Y.F. Xu, C.Y. Su, D.B. Kuang, Energy & Environmental Science, 7 (2014) 644-649.

[41] M. Lv, D. Zheng, M. Ye, L. Sun, J. Xiao, W. Guo, C. Lin, Nanoscale, 4 (2012) 5872-5879.

[42] N. Satoh, T. Nakashima, K. Kamikura, K. Yamamoto, Nature Nanotechnology, 3 (2008) 106-111.

[43] S. Monticone, R. Tufeu, A.V. Kanaev, E. Scolan, C. Sanchez, Applied Surface Science, 162 (2000) 565-570.

[44] C. Zheng, J. Liu, Q. Song, G. Dawson, C. Wei, Catalysis Communications, 21 (2012) 1–4.

[45] L. Liu, J. Qian, B. Li, Y. Cui, X. Zhou, X. Guo, W. Ding, Chemcal. Communication., 46 (2010) 2402-2404.

[46] H. Pan, J. Qian, A. Yu, M. Xu, L. Tu, Q. Chai, X. Zhou, Applied Surface Science, 257 (2011) 5059-5063.

[47] P.J. Holliman, M. Mohsen, A. Connell, M.L. Davies, M.J. Carnie, Journal of Materials Chemistry, 22 (2012) 13318-13327.

[48] C.Y. Jiang, X.W. Sun, G.Q. Lo, D.L. Kwong, J.X. Wang, Applied Physics Letters, 90 (2007) 547.

[49] Z.S. Wang, T. Yamaguchi, H. Sugihara, H. Arakawa, Langmuir the ACS Journal of Surfaces & Colloids, 21 (2005) 4272.

[50] M.K. Nazeeruddin, A. Kay, I. Rodicio, R. Humphrybaker, E. Mueller, P. Liska, N. Vlachopoulos, M. Graetzel, Journal of American Chemical Society, 115 (1993).

[51] A. Hagfeldt, M. Graetzel, Chemical Reviews, 95:1 (1995) 49-68.

[52] A. Hagfeldt, M. Grätzel, Accounts of Chemical Research, 33 (2000) 269.

[53] M. Grätzel, Progress in Photovoltaics Research & Applications, 8 (2000) 171–185.

[54] J. Yu, C. Zhang, Z. Jia, H. Qin, Q. He, Q. Liang, Chemical Research in Chinese Universities, 31 (2015) 412-417.